



Fut9 Deficiency Causes Abnormal Neural Development in the Mouse Cerebral Cortex and Retina

Asmaa Abdullah¹ · Yoshitaka Hayashi¹ · Naoko Morimura¹ · Akhilesh Kumar² · Kazuhiro Ikenaka² · Akira Togayachi³ · Hisashi Narimatsu³ · Seiji Hitoshi^{1,2}

Received: 25 March 2022 / Revised: 23 May 2022 / Accepted: 6 June 2022
© The Author(s), under exclusive licence to Springer Science+Business Media, LLC, part of Springer Nature 2022

Abstract

α 1,3-Fucosyltransferase 9 (*Fut9*) is responsible for the synthesis of Lewis X [Le^{X} , $\text{Gal}\beta$ 1-4($\text{Fuc}\alpha$ 1-3) GlcNAc] carbohydrate epitope, a marker for pluripotent or multipotent tissue-specific stem cells. Although *Fut9*-deficient mice show anxiety-related behaviors, structural and cellular abnormalities in the brain remain to be investigated. In this study, using in situ hybridization and immunohistochemical techniques in combination, we clarified the spatiotemporal expression of *Fut9*, together with Le^{X} , in the brain and retina. We found that *Fut9*-expressing cells are positive for *Ctip2*, a marker of neurons residing in layer V/VI, and *TLE4*, a marker of corticothalamic projection neurons (CThPNs) in layer VI, of the cortex. A birthdating analysis using 5-ethynyl-2'-deoxyuridine at embryonic day (E)11.5, 5-bromo-2'-deoxyuridine at E12.5, and in utero electroporation of a GFP expression plasmid at E14.5 revealed a reduction in the percentage of neurons produced at E11.5 in layer VI/subplate of the cortex and in the ganglion cell layer of the retina in P0 *Fut9*^{-/-} mice. Furthermore, this reduction in layer VI/subplate neurons persisted into adulthood, leading to a reduction in the number of *Ctip2*^{strong}/*Satb2*⁻ excitatory neurons in layer V/VI of the adult *Fut9*^{-/-} cortex. These results suggest that *Fut9* plays significant roles in the differentiation, migration, and maturation of neural precursor cells in the cortex and retina.

Keywords Fucosyltransferase · Neural stem cells · Retinal precursor cells · Migration · Corticothalamic projection neurons

Introduction

Carbohydrate epitopes of glycoproteins, glycolipids, and proteoglycans on the cell surface act as environmental sensors and play crucial roles in cell–cell interactions and signal transduction. Among them, Lewis X [Le^{X} ;

$\text{Gal}\beta$ 1-4($\text{Fuc}\alpha$ 1-3) GlcNAc , also known as stage-specific embryonic antigen-1 (SSEA-1) or leucocyte cluster of differentiation 15 (CD15) antigens] is a marker for pluripotent stem cells and is present on the inner cell mass of the mouse blastocyst and its derivative embryonic stem (ES) cells [1–4]. In addition, Le^{X} is expressed in tissue-specific precursor cells, for example, neural stem cells are enriched in a Le^{X} -positive population in adult mouse brains [5]. *Fut9* and *Fut10* are α 1,3-fucosyltransferases which play dominant roles in the synthesis of Le^{X} in the mouse brain [6, 7]. *Fut9* and *Fut10* are expressed in neural precursor cells in the ventricular zone (VZ) of embryonic mouse brains. While *Fut9* expression suppresses the self-renewal of neural stem cells in the cortex, *Fut10* expression enhances their self-renewal capability [7], suggesting that *Fut9* and *Fut10* possess apparently opposite functions in the maintenance of neural precursor cells, although these effects could be context-dependent [7–9].

In previous studies, *Fut9*-knockout mice were generated and revealed that *Fut9* deficiency resulted in the disappearance of Le^{X} antigens in the brain and mice exhibited

Kazuhiro Ikenaka Deceased.

✉ Yoshitaka Hayashi
yhayashi@belle.shiga-med.ac.jp

✉ Seiji Hitoshi
shitoshi-ty@umin.ac.jp

¹ Department of Integrative Physiology, Shiga University of Medical Science, Otsu 520-2192, Japan

² Department of Physiological Sciences, School of Life Sciences, The Graduate University for Advanced Studies, Okazaki 444-8787, Japan

³ Research Centre for Medical Glycoscience, Glycogene Function Team, National Institute of Advanced Industrial Science and Technology, Tsukuba 305-8568, Japan

increased anxiety-like responses in dark–light preference and in elevated plus maze tests [10, 11]. In addition, genome-wide association studies of neuropsychiatric disorders repeatedly detected *Fut9* as a risk gene for schizophrenia [12–16]. However, the brain structure and cellular bases for these anxiety-related behaviors remain largely unclarified because only a marginal decrease in the number of calbindin-positive neurons in the basolateral amygdala was detected in adult *Fut9*^{-/-} mice [11]. Our previous study revealed that *Fut9* deficiency enhances the self-renewal of cortical neural stem cells [7], which could suppress or delay their differentiation. Neurons are generated from neural precursor cells and radially migrate in the developing cortex in a birth date-dependent inside-out fashion to yield the elaborate layered structure. Therefore, it is possible that the delay of precursor cell differentiation in *Fut9*^{-/-} embryonic brains could result in, as yet unidentified structural changes in the postnatal brain layers.

In this study, we focused on the brain and retina, the latter of which is derived from the optic vesicle that forms from laterally projecting bulges from the forebrain, in the embryonic and postnatal mouse brain and found abnormalities in the differentiation of neural and retinal precursor cells.

Materials and Methods

Mice and Genotyping

CD1 (ICR) mice were used, and all mice were kept in the institution's Research Center for Animal Life Science with a 12:12 h light–dark cycle (8 am–8 pm) and unlimited access to food and water. Noon of the plugged date was considered to be embryonic day (E) 0.5 and the day of birth as postnatal day (P) 0. Mice heterozygous for *Fut9* [10] were maintained on the CD1 background. DNA was obtained from the tip of the tail and mutant mice were genotyped by PCR, using *fut9_A1* (5'-TGAGCATGCCAGGGTCAAGTAT-3'), *CB341R* (5'-CATGTGATTCCCAAACCG-3') and *fut9_KO_R3* (5'-GCCATGATGGATACTTTCT-3') primers. Target DNA was amplified for 35 cycles in a thermal cycler with denaturation at 95 °C for 30 s, annealing at 58 °C for 30 s, and extension at 68 °C for 30 s. All experimental procedures were approved by the institution's Animal Research Committee.

In Situ Hybridization (ISH) and Immunohistochemistry

DNA fragments used to generate ISH probes were amplified by PCR using *fut9_F1* (5'-CCACACCTATGGCCAAGC ATTC-3') and *fut9_R1* (5'-GCTCCCCTTCACAAATGT GGTAC-3') primers for *Fut9* and *grin1_F1* (5'-ACGGGG

CCTAATGACACA-3') and *grin1_R1* (5'-ATGGCCTCA GCTGCACTC-3') primers for *Grin1*. The ISH probe for *Fut9* is localized within exon 3 that is deleted in the mutant allele. DNA fragments were cloned into the pBlueScript II SK (+) plasmid and digoxigenin (DIG)-labeled single-stranded sense or anti-sense riboprobes were synthesized using T3 or T7 RNA polymerase and DIG RNA labeling mix (Roche).

Coronal cryosections at 14 µm thickness made from the head of embryos and P0 pups included the brain and retina, and coronal cryosections at 20 µm thickness were made from the adult brain. ISH and immunohistochemistry were performed as described previously [17]. Briefly, cryosections were treated with proteinase K (1 µg/ml, 60–90 min, room temperature), and then hybridized with sense or antisense DIG-labeled RNA probes at 65 °C overnight. The hybridized DIG-labeled RNA probes were detected by alkaline phosphatase conjugated anti-DIG antibody (1:2000, 11093274910, sheep polyclonal IgG, Roche) and visualized by incubation of the sections with an alkaline phosphatase substrate (nitro blue tetrazolium/5-bromo-4-chloro-3-indolyl phosphate; NBT-BCIP; Nacalai Tesque).

Co-detection by ISH and immunohistochemistry were performed as usual for ISH but without proteinase K treatment, followed by immunostaining. After detection with NBT-BCIP, sections were incubated with primary antibodies for Ctip2 (Abcam, ab18465, rat monoclonal IgG Clone 25B6, 1:100), TLE4 (Santa Cruz, sc-365406, mouse monoclonal IgG Clone E-10, 1:100), *Satb2* (Abcam, ab34735, rabbit polyclonal IgG, 1:100), SSEA-1 (R&D Systems, MAB2155, mouse monoclonal IgM Clone MC-480, 1:100), 5-bromo-2'-deoxyuridine (BrdU; Millipore, MAB4072, mouse monoclonal IgG clone 131–14871, 1:500), and GFP (Life Technologies, A6455, rabbit polyclonal IgG, 1:1000) then visualized using Alexa Fluor 488-, 555- or 647-conjugated secondary antibodies (Invitrogen). 5-Ethynyl-2'-deoxyuridine (EdU) visualization was conducted using the Click-iT EdU imaging kit (Invitrogen) according to the manufacturer's instructions. Cell nuclei were counterstained with Hoechst33342 (1 µg/ml; Sigma). For immunostaining of Ctip2, TLE4, and *Satb2*, the cryosections were boiled in a microwave for 5 min in 10 mM citrate buffer, pH 6.0.

Birthdating Analysis and in Utero Electroporation

For birthdating analysis of neurons, pregnant mice were intraperitoneally injected with EdU (50 mg/kg) at E11.5 followed by BrdU (50 mg/kg) at E12.5, prior to in utero electroporation. In utero electroporation was performed as described previously [18]. E14.5 pregnant CD1 mice were deeply anesthetized by intraperitoneal injection of ketamine (100 mg/kg body weight) and xylazine (10 mg/kg). The mixture of pCX-GFP (3 µg/µl), a GFP expression plasmid, in

PBS with 0.1% Fast Green was microinjected into the lateral ventricle of the E14.5 embryo brain and plasmid was electroporated using an electroporator (NEPA21, NEPA GENE) with five 50 ms pulses of 35 V at 950 ms intervals. The pCX-GFP plasmid-electroporated embryos from the EdU and BrdU injected dam were sacrificed at P0 and three or more *Fut9*^{-/-} and littermate control pups were analyzed. The number of EdU⁺, BrdU⁺ and GFP⁺ cells in the cortex was counted for each brain layer, which were identified by the expression of *Ctip2*, a marker for layer V/VI. The counts from five sections for each brain were averaged.

Flow Cytometry

Nuclei isolation, nuclei counting, and nuclei immunostaining of cells from the cortex of *Fut9*^{-/-} and littermate control mice were performed as described previously [19]. Flow-Count® (Beckman Coulter) was used to count the total number of nuclei, then nuclei were immunostained against *Ctip2* and *Satb2*. Isotype control IgG was used as a negative control for each (rabbit IgG, Southern Biotech, 0111-01; rat anti-GFP IgG2a, 04404-84, Nacalai Tesque). Flow cytometry data were analyzed by FlowJo™ (Becton, Dickinson & Company).

RNA-Sequencing Analysis from a Public Database

Raw RNA-sequencing data were downloaded from the NCBI Gene Expression Omnibus (accession number: GSE63482) and were analyzed following the original report [20]. Pair-end reads were mapped to the *Mus musculus* genome (mm10) using Tophat2 [21]. Mapped reads were counted and annotated based on the *Mus musculus* genome assembly GRCm38 (mm10) using featureCount [22] with default settings. Gene-level and transcript counts were then imported into R/Bioconductor package EdgeR [23] and were normalized for TMM (trimmed mean of M-values) to adjust for differences in library size. A heatmap from analyzed expression values was made using GraphPad PRISM™ (GraphPad Software, Inc., San Diego, CA).

Statistics

Statistical analysis was performed using unpaired two-tailed Student's *t*-test using GraphPad PRISM™ with the level of significance set at $p < 0.05$.

Results

Spatiotemporal Expression of *Fut9* and *Le.X* in the Developing Cortex and Retina

First, we examined the expression of *Fut9* by ISH in the brain and retina of early- to late-stage mouse embryos. In the developing cortex, neurons are generated from neural precursor cells and radially migrate in a birth date-dependent inside-out fashion. After the first production of subplate neurons in the subplate (SP) and Cajal-Retzius cells in the marginal zone (MZ), early-born neurons settle in the deep layer, and later-born neurons migrate beyond the early-born neurons using radial glia-guided locomotion to add subsequent upper layers [24]. Ultimately, the SP becomes the

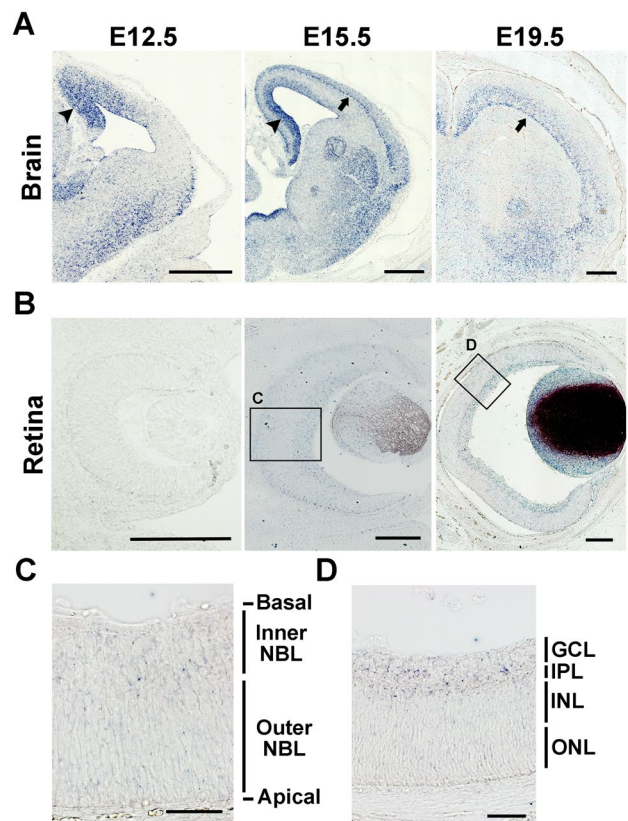


Fig. 1 Coronal cryosections of the developing mouse brain (A) and retina (B) at E12.5, E15.5, and E19.5 were analyzed for *Fut9* expression using in situ hybridization. *Fut9* signals were detected in the dorsomedial portion of the VZ/SVZ (arrowheads in A) and the cortical layer (arrows in A) in the brain and in the basal part of the retina at E15.5 and E19.5 but not at E12.5. C and D The boxed areas shown in the E15.5 and E19.5 retina in (B) are shown at higher magnification. The *Fut9* signals were detected in the inner neuroblast layer (NBL) of the E15.5 retina (C) and in the ganglionic cell layer (GCL) and inner plexiform layer (IPL) of the E19.5 retina (D). Scale bars: 400 μm (A), 200 μm (B), and 50 μm (C and D)

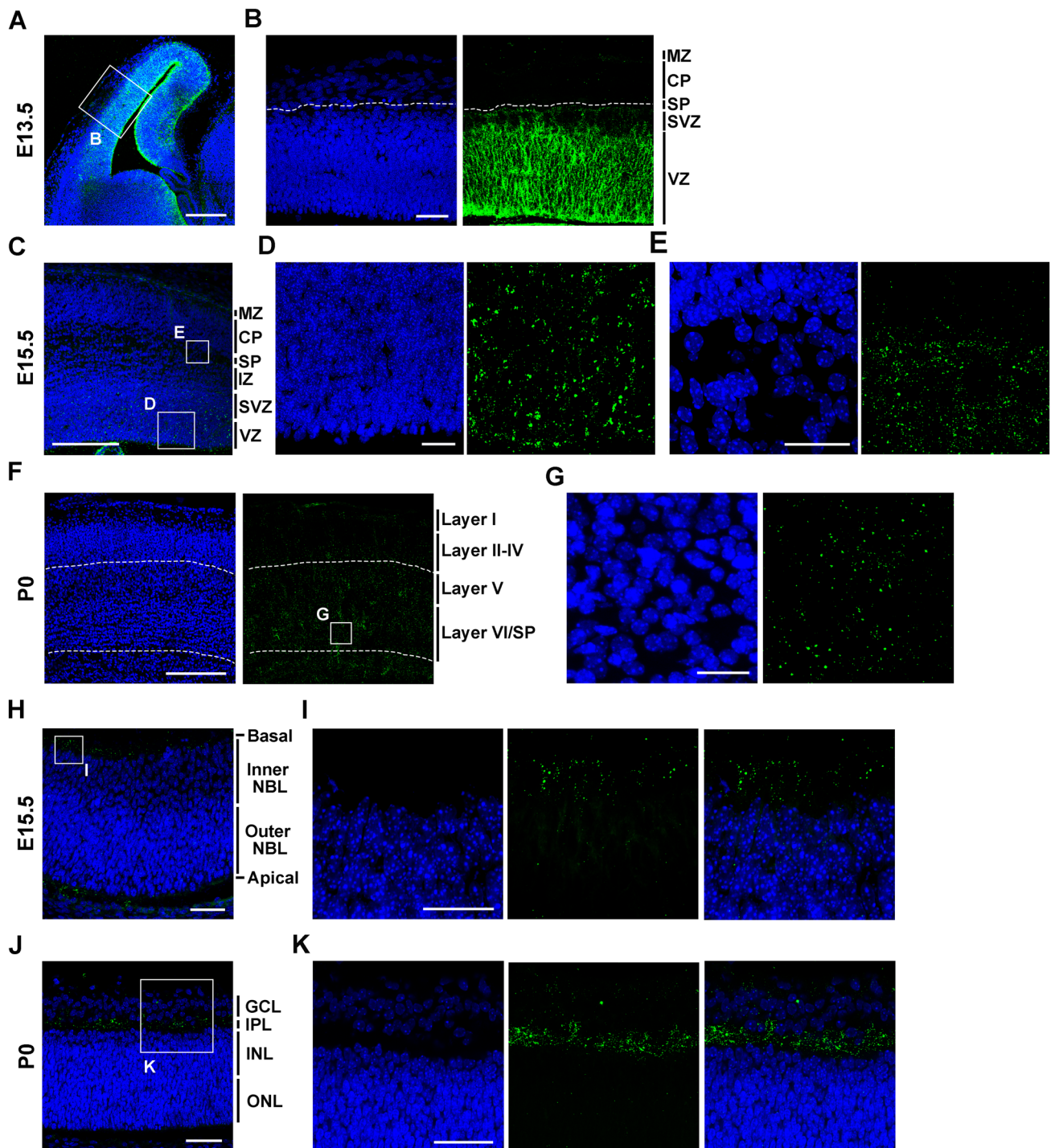


Fig. 2 Lewis X antigens in the developing cortex (**A**, **C**, and **F**) and retina (**H** and **J**) were immunostained using an anti-SSEA-1 antibody at the indicated time points. **A**, **B** SSEA-1 immunoreactivity was present in the VZ/SVZ of the E13.5 cortex. The boxed area in (**A**) is shown at higher magnification (**B**). **C–E** The boxed areas from the E15.5 cortex in (**C**) are shown at higher magnification, appearing as stronger punctate signals in the VZ/SVZ (**D**) and weaker punctate signals in the intermediate zone (IZ) and subplate (SP), but not in the cortical plate (CP) nor marginal zone (MZ) of the cortex (**E**). **F** and

G The boxed area from the P0 cortex in (**F**) is shown at higher magnification (**G**), and the abundant SSEA-1 signals in layer VI/SP and layer V are evident. **H–K** The boxed areas from the E15.5 (**H**) and P0 (**J**) retina are shown at higher magnification (**I**) and (**K**), respectively, with clear signals in the basal-most area of the E15.5 inner neuroblast layer (NBL) (**I**) and in the inner plexiform layer (IPL) and ganglion cell layer (GCL) (**K**). INL: inner nuclear layer, ONL: outer nuclear layer. Scale bars: 200 μm (**A**, **C**, and **F**), 50 μm (**B**, **H**, **J**, and **K**), and 25 μm (**D**, **E**, **G**, and **I**)

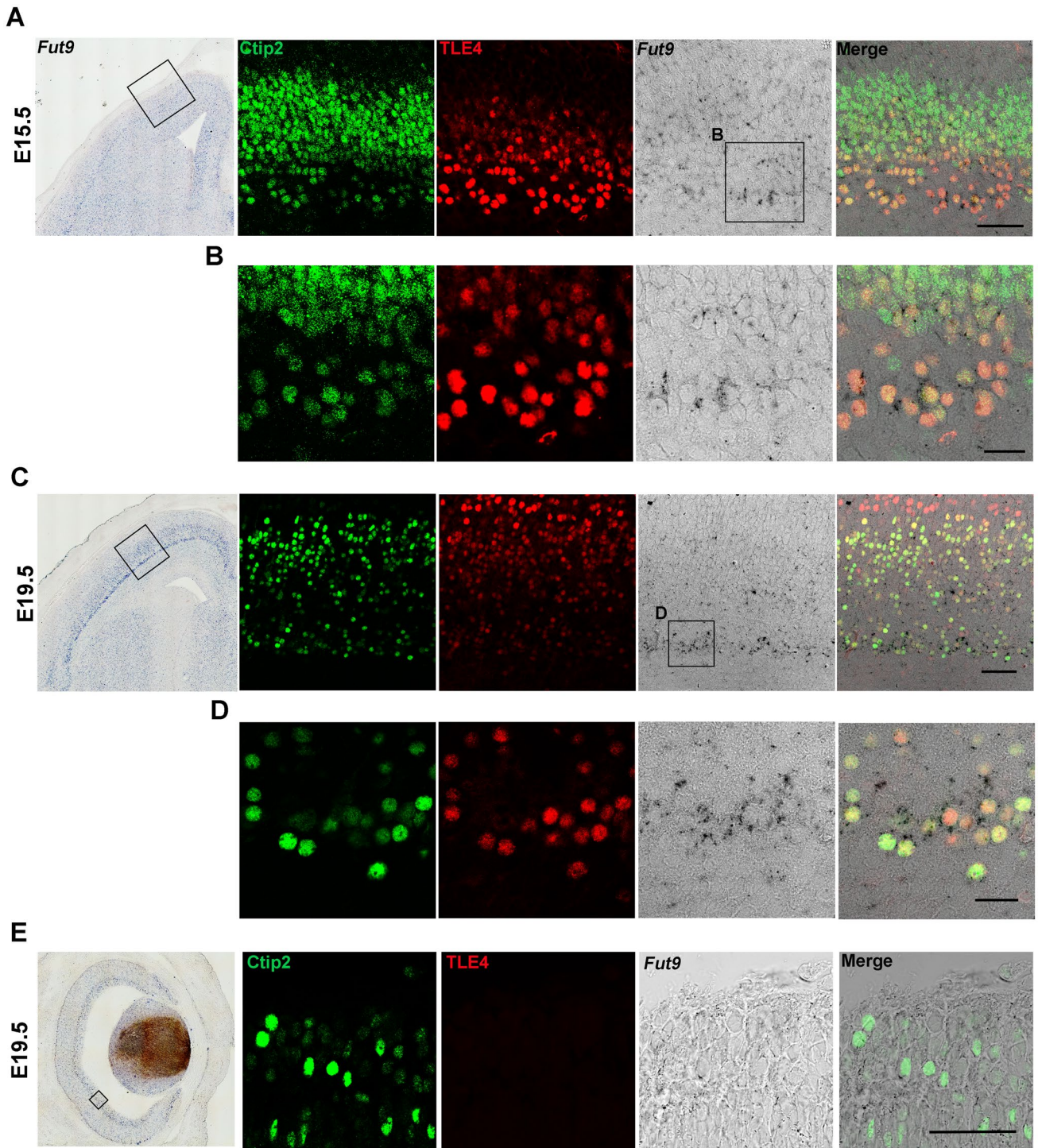
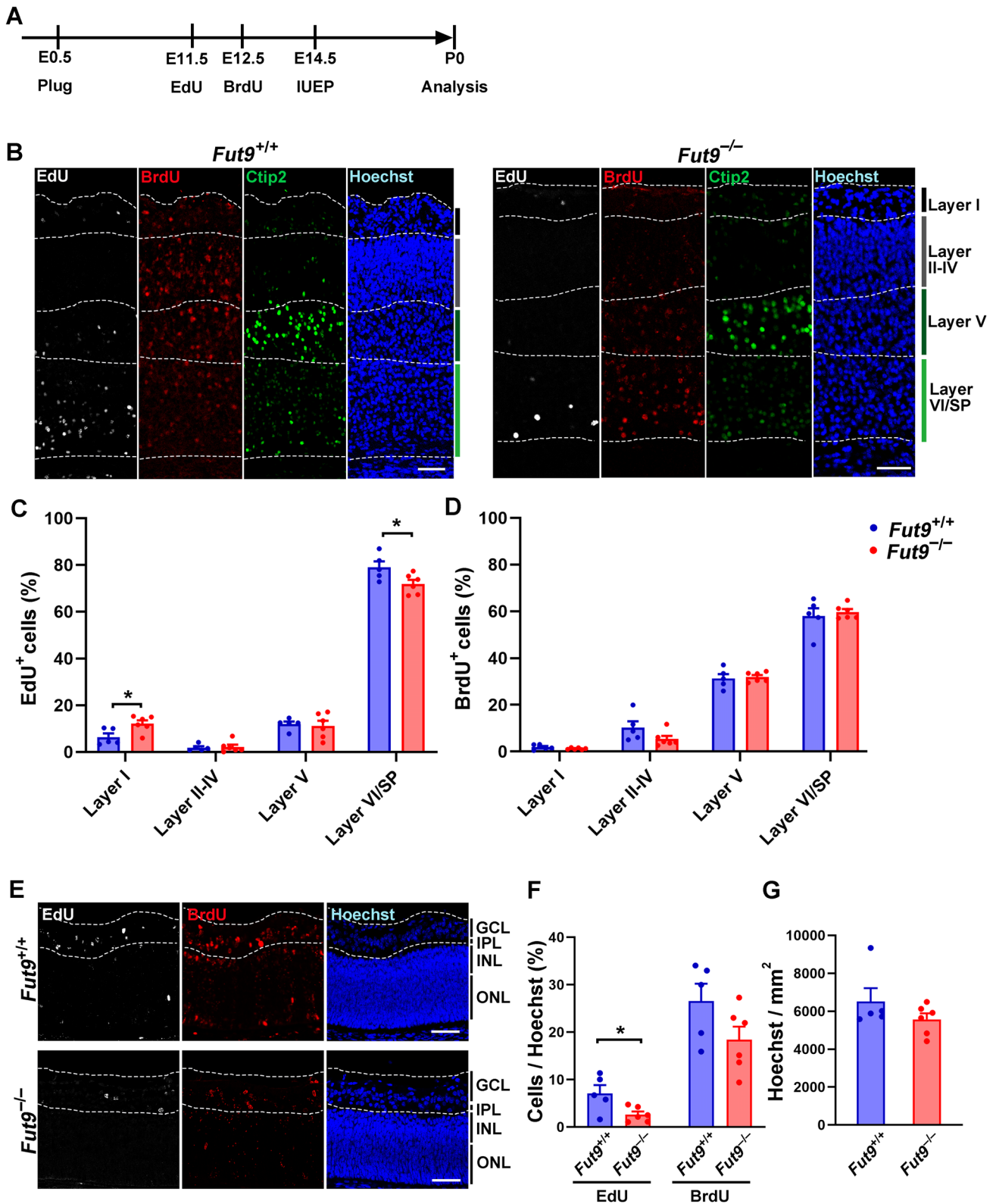


Fig. 3 Co-detection of *Fut9* expression using in situ hybridization followed by immunostaining for Ctip2 and TLE4 in the E15.5 (A) and E19.5 (C) cortex and E19.5 retina (E). The boxed areas in the left panels are shown at higher magnification at right (A, C, and E). *Fut9* signals are present in the Ctip2- and TLE4-positive layer of the E15.5 (A) and E19.5 (C) cortex. The boxed areas in the *Fut9* signal images

(A and C) are shown at even higher magnification (B and D), demonstrating the co-localization of *Fut9* signals and Ctip2 and TLE4 immunoreactivity in the deep layer of the cortex. E *Fut9* signals are detected in the Ctip2-positive region in the ganglionic cell layer of the E19.5 mouse retina. Scale bars: 50 μm (A, C, and E) and 20 μm (B and D)



bottom part of layer VI and the MZ becomes layer I, resulting in the formation of six layers in the postnatal brain. *Fut9* was abundantly expressed in the dorsomedial portion of the

ventricular zone/subventricular zone (VZ/SVZ) of the E12.5 cortex, which disappeared towards E19.5 (Fig. 1A). Strong *Fut9* ISH signals also emerged in the upper cortical layer of

Fig. 4 (A) Timeline for the birthdating analysis. Newborn neurons were labeled with EdU at E11.5, then with BrdU at E12.5. **B** and **E** Immunostaining of EdU and BrdU in the cortex (**B**) and retina (**E**) from P0 *Fut9^{+/+}* and *Fut9^{-/-}* mice. **B** Cortical layers were identified by Ctip2 immunostaining and nuclei staining (dotted lines). **C** and **D** Bar graphs show percentages of EdU⁺ (**C**) and BrdU⁺ (**D**) cells in each layer of the cortex from *Fut9^{-/-}* and littermate control mice. **F** Percentages of EdU⁺ and BrdU⁺ cells were calculated against the total number of Hoechst33342⁺ cells in the ganglion cell layer (GCL). **G** The density of Hoechst33342⁺ cells in the ganglionic cell layer from P0 *Fut9^{-/-}* and littermate control retina was normalized by area. IUEP: in utero electroporation. * $p < 0.05$ by Student's *t*-test. Data represent means \pm SEM. Scale bars: 100 μ m (**B**) and 50 μ m (**E**)

the E15.5 brain, which persisted as expression in the deep layer of the E19.5 cortex (Fig. 1A). Conversely, ISH signals for *Fut9* were completely absent in the *Fut9^{-/-}* brains (Supplementary Fig. 1). Although *Fut9* expression was below the level of detection in the neural retina, a derivative of neuroepithelium, at E12.5, the expression was detectable beginning and after E15.5 (Fig. 1B). The developing mouse retina consists of two layers; the inner neuroblast layer (NBL), which contains postmitotic differentiating cells, and the outer NBL, in which mitotic retinal precursor cells reside. *Fut9* expression was restricted to the inner NBL at E15.5 and the ganglion cell layer (GCL) and inner plexiform layer (IPL) at E19.5 in the retina (Fig. 1C, D). These results suggest that although *Fut9* is expressed in the neural precursor cells in the cortex at early to middle embryogenesis, its expression shifts to postmitotic neurons in the brain and retina during late embryonic stages in mice.

We next investigated the expression of SSEA-1 in the mouse brain and retina by immunohistochemistry. As expected from the results of *Fut9* expression, strong SSEA-1 immunoreactivity was observed in the VZ/SVZ of the E13.5 cortex (Fig. 2A, B) and weaker signals were detected in the subplate (SP) of the E15.5 cortex (Fig. 2C–E) and in layer V and layer VI/SP of the P0 cortex (Fig. 2F, G). SSEA-1 immunoreactivity was also detected in the basal most area of the inner NBL in the E15.5 retina (Fig. 2H, I), which becomes more prominent in the IPL of the P0 retina (Fig. 2J, K). To verify these patterns of immunoreactivity, we examined the brain and retina from *Fut9^{-/-}* embryos and found that SSEA-1 immunoreactivity was completely absent (Supplementary Fig. 2). Thus, our observations confirmed that *Fut9* dominantly synthesizes Le^X antigens recognized by an anti-SSEA-1 antibody in the developing mouse brain and retina.

Specification of *Fut9*-Expressing Cells in the Brain and Retina

Since *Fut9* is strongly expressed in specific layers in the brain and retina, we characterized *Fut9*-expressing cells in

these layers using co-detection via ISH and immunohistochemistry in embryos at E15.5 and E19.5. Following ISH for *Fut9*, sections were immunostained for Ctip2, a marker for layer V/VI, and TLE4, a marker for corticothalamic projection neurons (CThPNs) which mostly reside in layer VI. *Fut9* signals were observed in the upper cortical layer of the E15.5 cortex (Fig. 3A) and in layer V/VI of the E19.5 cortex (Fig. 3C), where the *Fut9* signals closely surrounded Ctip2 and TLE4 double-positive nuclei (Fig. 3B, D). In contrast, although TLE4 is absent from the retina, *Fut9* signals colocalized with Ctip2⁺ nuclei in the GCL of the E19.5 retina (Fig. 3E). These results suggest that *Fut9* is expressed in Ctip2⁺ cells, including, at least in part, corticothalamic projection neurons in layer V/VI of the brain and Ctip2⁺ cells in the GCL of the retina.

Fut9 Deficiency Impaired the Generation of Early-Born Neurons

Neurons in layer V/VI of the cortex are generated in the earliest stage of neurogenesis during E11.5–12.5, after the production of Cajal-Retzius cells. We, therefore, investigated whether *Fut9* deficiency affects the generation and migration of layer V/VI neurons by labeling proliferating neural progenitor cells with nucleotide analogues, EdU and BrdU (Fig. 4A). While undifferentiated neural precursor cells that have incorporated nucleotide analogues eventually dilute the label to below the detection limit after several rounds of division, precursor cells that undergo postmitotic differentiation immediately after analogue incorporation retain the label as they migrate to their final destinations. Therefore, by immunostaining for the analogue label in neurons, we could determine the birthdates of those neurons. In addition, we labeled the dorsal VZ of the cortex by electroporating GFP expression plasmids at E14.5 and analyzing the cortex and retina from P0 pups (Fig. 4A).

As expected, EdU⁺ neurons that had been born at or shortly after E11.5 were mostly present in layer VI/SP in the P0 cortex (Fig. 4B) and fewer EdU⁺ neurons were observed in the layer VI/SP of *Fut9^{-/-}* brains as compared to littermate controls ($t_{(9)} = 2.402$, $p = 0.0398$) (Fig. 4C). In contrast, we could find no significant differences in the distribution of BrdU⁺ neurons that had been born at or shortly after E12.5 (Fig. 4D) nor in GFP⁺ neurons that had been born at or shortly after E14.5 (Supplementary Fig. 3). The retinal progenitor cells reside in the most apical part of the retinal neuroepithelium and generate six types of neurons and Müller glia, which migrate to the upper layers at E11.5 and beyond [25]. Ganglion, horizontal, amacrine, and cone cells are generated first, then bipolar and rod cells and Müller glia differentiate later. Both EdU⁺ early-born and BrdU⁺ later-born neurons were detected in the GCL of the retina from P0 pups (Fig. 4E). We found a statistically significant

decrease in the number of EdU⁺ neurons and a non-significant decrease of BrdU⁺ neurons in *Fut9*^{-/-} retina compared to littermate controls ($t_{(9)} = 2.630$, $p = 0.0274$ for EdU; $t_{(9)} = 1.814$, $p = 0.1030$ for BrdU; Fig. 4F), although total cell numbers were comparable between *Fut9*^{-/-} and control mice [$t_{(9)} = 1.274$, $p = 0.2347$; Fig. 4G].

Excitatory Projection Neurons in the Deep Layer of the Adult Cortex were Reduced in *Fut9*^{-/-} Brains

To determine if the reduction of early-born neurons found in layer VI/SP of P0 *Fut9*^{-/-} pups persisted into adulthood, we performed flow cytometry analysis by which cells can be classified depending on the levels of fluorescence. We used the cortex from 8-week-old mice and immunostained isolated cortical nuclei for Ctip2 and Satb2, a marker of layers II–VI. We found that the nuclei could be divided into Ctip2⁺ and Ctip2⁻ populations and that the Ctip2⁺ population could be further divided into Ctip2^{strong} and Ctip2^{weak} subpopulations (Fig. 5A, B and Supplementary Fig. 4A–C). The cells could also be divided into Satb2⁺ and Satb2⁻ populations; thus, the cells could be classified into 6 groups (Fig. 5A and Supplementary Fig. 4D). Among them, we found fewer cells in the Ctip2^{strong}/Satb2⁻ subpopulation in the cortex of *Fut9*^{-/-} compared to littermate *Fut9*^{+/-} mice (Fig. 5C and Supplementary Fig. 4).

We next tried to localize Ctip2^{strong}/Satb2⁻ cells in the cortex using immunohistochemical methods (Fig. 5D–F) and classifying cells into three groups (Ctip2^{strong}, Ctip2^{weak} and Ctip2⁻), although it was difficult to precisely correlate the results of immunohistochemistry to those of flow cytometry. Based on the histochemical analysis, we counted cell numbers in each group in layers IV, V, and VI (Fig. 5F). The data are shown as pie charts; layer IV was dominated by Ctip2⁻ cells and layer V was a mixture of Ctip2^{strong} and Ctip2⁻ cells (Fig. 5G). Layer VI could be divided into the upper and lower sublayers based on the cell components; the upper layer VI contained Ctip2⁻ cells but the lower layer VI was devoid of Ctip2⁻ cells (Fig. 5G). Only Satb2^{strong} and Satb2^{weak} cells, but no Satb2⁻ cells, were observed in layers V and VI, which prompted us to consider that Ctip2^{strong}/Satb2^{weak} cells, as detected by immunohistochemistry, mostly corresponded to the Ctip2^{strong}/Satb2⁻ subpopulation selected by flow cytometry. Our data suggest that Ctip2^{strong}/Satb2^{weak} neurons in layer V/VI of the adult cortex were decreased in the *Fut9*^{-/-} mice (Fig. 5C and Supplementary Fig. 5), which is consistent with the EdU birthdating analysis in P0 pups.

We then asked if the Ctip2^{strong}/Satb2^{weak} neurons in layer V/VI were excitatory or inhibitory. RNA sequencing data from two replicated experiments showed that

subcerebral projection neurons (ScPNs) in layer V have a profile of Ctip2^{high}, TLE4^{low}, and Satb2^{low}, whereas CThPNs in layer VI possess a profile of Ctip2^{moderate}, TLE4^{high}, and Satb2^{low} [20]. Both ScPNs and CThPNs abundantly express genes associated with excitatory neurons (Fig. 6A). Among those excitatory marker genes, we selected *Grin1*, encoding NMDA-type glutamate receptor subunit zeta-1, and performed ISH for *Grin1*, followed by Ctip2 and Satb2 immunostaining (Fig. 6B–E). ISH signals were detected surrounding Ctip2^{strong}/Satb2^{weak} neurons in layer VI/SP of P0 brains as well as in layer V/VI of the adult cortex (Fig. 6C, E). These results suggest that the early-born neurons, which were reduced in the *Fut9*^{-/-} brains, were excitatory projection neurons.

Discussion

Since Le^X is a well-known marker for undifferentiated ES cells and is also expressed in neurosphere-forming neural stem cells [1–5], it had been generally believed that *Fut9* deficiency should result in the loss of neural stem cell maintenance. However, contrary to belief, our previous study showed that the self-renewal capability of neural stem cells in the dorsal portion of the VZ is actually enhanced in the absence of *Fut9* [7]. Our results appear inconsistent with the study by Yagi et al. [8], showing that the knockdown of *Fut9* in neural stem cells reduced neurosphere formation through the attenuation of Notch signaling. This discrepancy may result from differences in the source of the neural stem cells; we used cortical neural stem cells, which abundantly express *Fut9*, and Yagi et al. used neural stem cells from the ganglionic eminence. Indeed, we could not detect any effects of *Fut9* deficiency on the self-renewal of neural stem cells from the medial ganglionic eminence [7]. Le^X is also synthesized by *Fut10*, which is expressed throughout the entire VZ of embryonic mouse brains, although *Fut10* requires strict substrate specificities [7]. Therefore, it is possible that anti-Le^X antibody-mediated enrichment of neural stem cells [5, 26] is mediated by *Fut10*-synthesizing Le^X, however, we could not rule out the contribution of scarce expression of *Fut9*. Although the precise mechanisms governing how Le^X affects the maintenance and differentiation of neural precursor cells remain largely unknown, it was recently reported that bone morphogenetic protein induces the expression of Le^X and this, in turn, promotes cell cycle withdrawal [27].

The enhanced self-renewal of cortical neural stem cells by *Fut9* deficiency predicts the delay in neuronal differentiation from neural precursor cells, leading to an altered distribution of their progeny. Indeed, our current study examined the spatiotemporal profile of neural precursor cell differentiation and revealed a reduction of early-born neurons that would eventually reside in the deep layers of

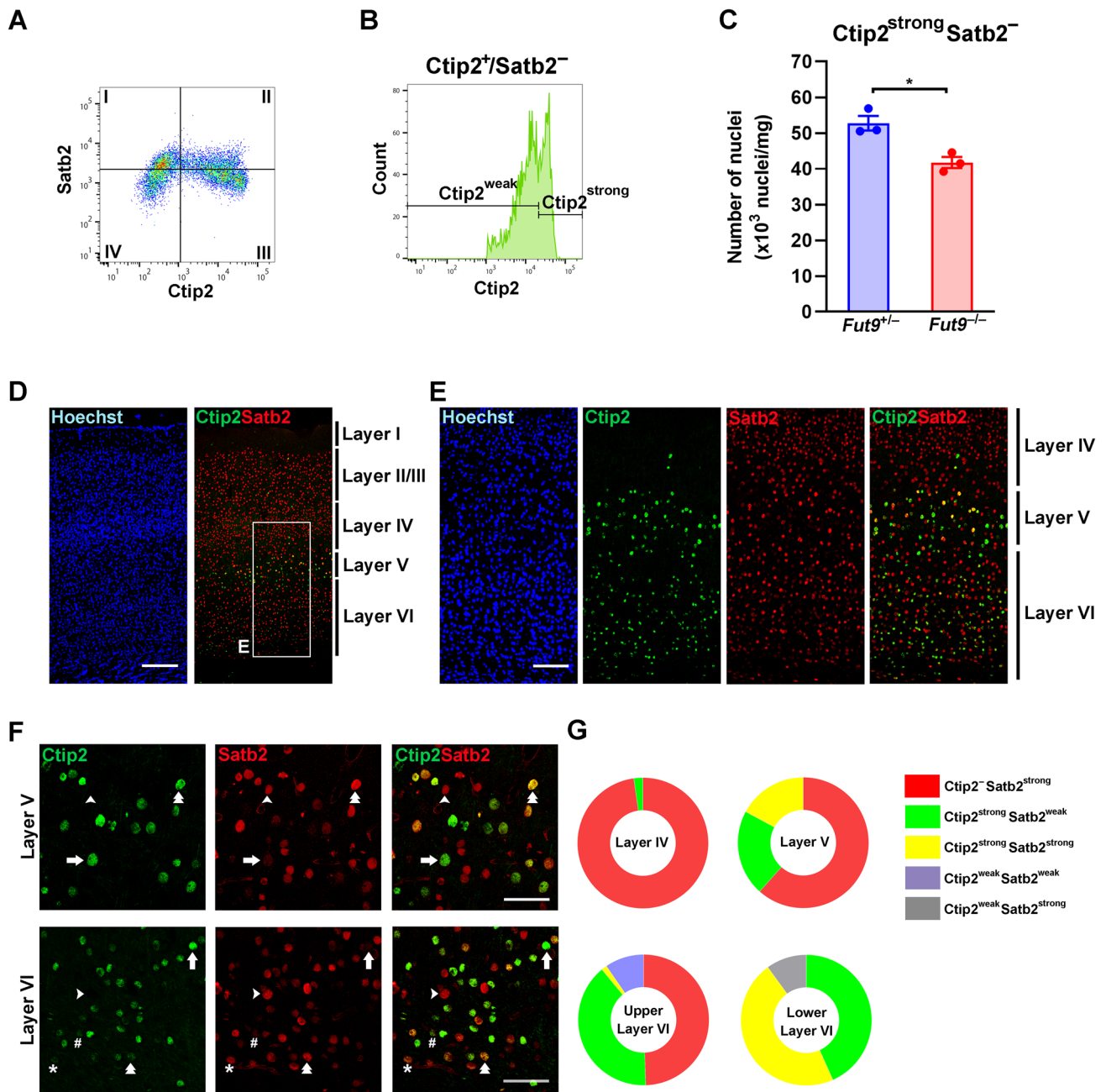


Fig. 5 A–C Flow cytometry analysis of Ctip2- and Satb2-immunoreactive cells in the cortex from adult *Fut9*^{-/-} and littermate control mice. **A** The density plot shows four populations: Ctip2⁻/Satb2⁺ (I), Ctip2⁺/Satb2⁺ (II), Ctip2⁺/Satb2⁻ (III), and Ctip2⁻/Satb2⁻ (IV). **B** A histogram of the Ctip2⁺/Satb2⁻ population shows two peaks corresponding to distinct populations of Ctip2^{strong} and Ctip2^{weak} nuclei. **C** The bar graph shows the number of Ctip2-strong positive and Satb2-negative nuclei from the cortex of *Fut9*^{-/-} and littermate control mice. **D–F** Ctip2 and Satb2 immunostaining of the adult mouse cortex. The

boxed area in **(D)** is shown at higher magnification in **(E)**. **F** Layer V and VI are shown at even higher magnification. The distinct immunoreactivity profiles are shown as follows: Ctip2^{strong}/Satb2^{weak} (arrows), Ctip2⁻/Satb2^{strong} (arrowheads), Ctip2^{strong}/Satb2^{strong} (double arrowheads), Ctip2^{weak}/Satb2^{weak} (#) and Ctip2^{weak}/Satb2^{strong} (*). **G** Pie charts for each subpopulation with distinct immunoreactivity profiles against Ctip2 and Satb2 in layer IV, layer V and upper and lower layer VI. **p* < 0.05 by Student's *t*-test. Data represent means ± SEM. Scale bars: 200 μm (**D**), 100 μm (**E**), and 50 μm (**F**)

the adult cortex. Those *Fut9*-expressing early-born neurons are likely excitatory projection neurons although their cell identities should be further characterized. In addition, it remains to be determined where the *Fut9*-expressing

neurons send axons and whether or not *Fut9*-deficient excitatory projection neurons in the deep layer form appropriate connections with other neurons. Interestingly, post-mortem studies of the brain from schizophrenia patients

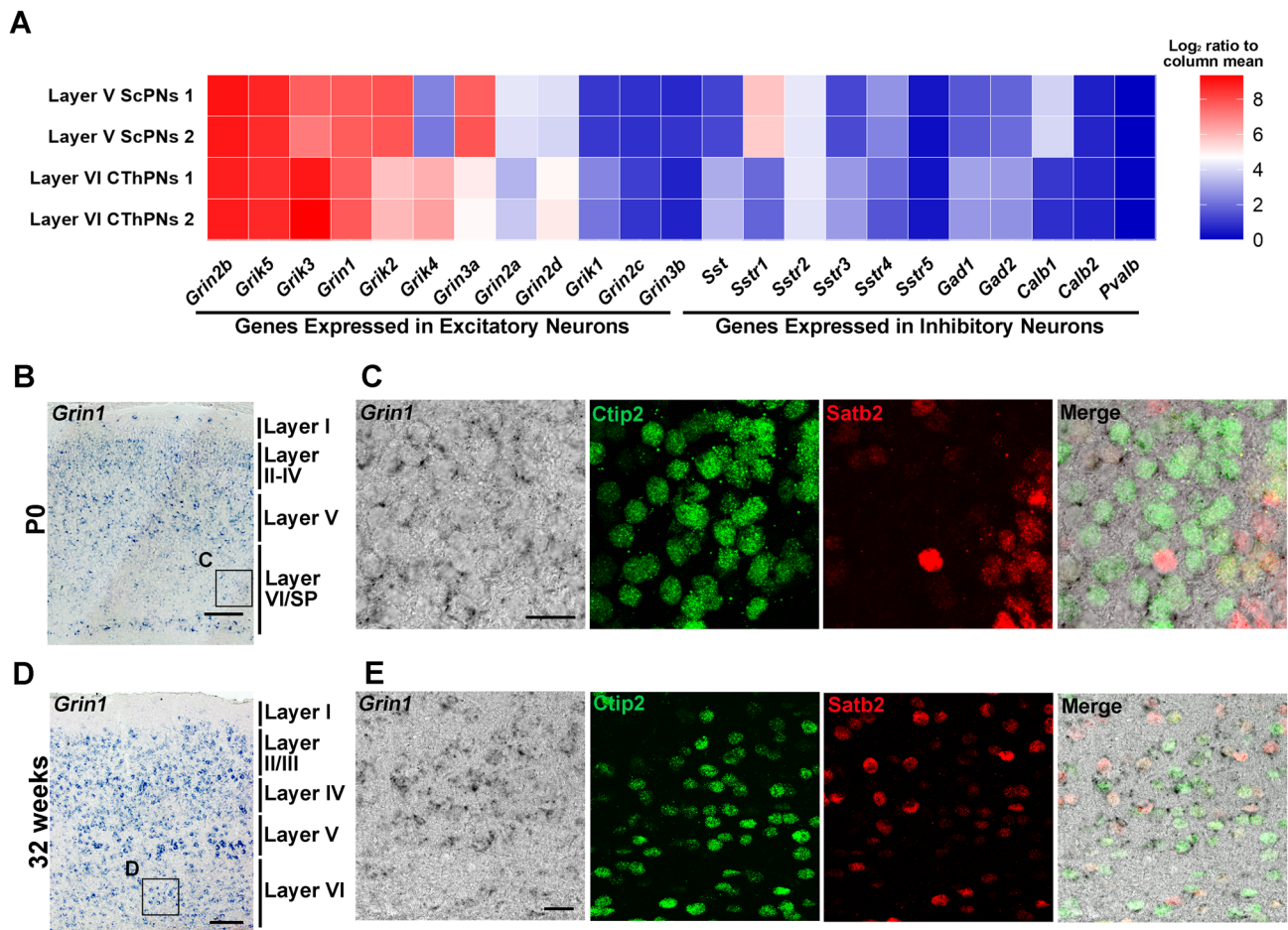


Fig. 6 **A** The heatmap of gene expression levels for layer V subcortical projection neurons (ScPNs) and layer VI corticothalamic projection neurons (CThPNs) from the public replicated RNA-sequencing database reported by Molyneaux et al. [20] shows genes expressed in excitatory and inhibitory neurons. **B–E** *Grin1* expression was detected by in situ hybridization, followed by immunostaining for

Ctip2 and *Satb2*, in the P0 (**B**) and adult (**D**) mouse cortex. The boxed areas in the *Grin1* signal images in (**B**) and (**D**) are shown at higher magnification in (**C**) and (**E**), respectively. *Grin1* mRNA signals were detected surrounding *Ctip2*⁺/*Satb2*^{weak} nuclei. Scale bars: 100 μ m (**B** and **D**) and 20 μ m (**C** and **E**)

have revealed alterations in the number of neurons and soma size in the deep layers of the cortex [28, 29]. The increased anxiety-like behaviors observed in *Fut9*^{-/-} mice could be mediated, at least in part, by the reduction in early-born projection neurons, although further investigation is required to show a causative link between them.

The early-born neurons, which were reduced in the *Fut9*^{-/-} retina, localize to the GCL and are likely retinal ganglion cells. On the other hand, it has been reported that Le^X-positive neurons in the postnatal retina are mostly amacrine cells [30], which is consistent with our observations that SSEA-1 immunoreactivity is visible in the inner plexiform layer, where amacrine cells send their neurites. We also detected a few SSEA-1-immunoreactive cells in the wild-type GCL. However, it is currently unknown whether these neurons are lost or whether they survive

but lose SSEA-1-immunoreactivity in the *Fut9*^{-/-} retina. Although the ISH signals for *Fut9* were below detection limits in the E12.5 retina, it is still possible that marginal expression of *Fut9* in the retina is sufficient and critical for the differentiation of early-born neurons or, alternatively, *Fut9* deficiency could reduce the survival of these neurons during later stages. It would be intriguing to perform visual cue-dependent behavioral tests to reveal if there are functional and structural differences between early-born and late-born retinal ganglion cells.

Supplementary Information The online version contains supplementary material available at <https://doi.org/10.1007/s11064-022-03651-8>.

Acknowledgements The authors thank Dr. Natsu Koyama (Shiga University of Medical Science) for her advice on this research and also thank Ms. Mariko Tomoeda, Ms. Masako Mori and all staff of the

Research Center for Animal Life Science and Central Research Laboratory at Shiga University of Medical Science for their technical support.

Author Contributions All authors contributed to the study conception and design. Material preparation, data collection and analysis were performed by AA and YH. The manuscript was written by AA, YH and SH, and all authors commented on it. All authors read and approved the final version of the manuscript except for KI, who passed away during the study.

Funding This work was supported by Grants-in-Aid for Scientific Research (B) (Grant No. 16H04671) (S. H.) and Research (C) (Grant No. 20K07758) and Grants-in-Aid for Young Scientists (Grant No. 26870282, 17K17815) (Y. H.) from the Ministry of Education, Culture, Sports, Science and Technology of Japan, a Grant from SENSHIN Medical Research Foundation (S.H.), Grants from THE FUGAKU TRUST FOR MEDICINAL RESEARCH and from the Brain Sciences Project of the Center for Novel Science Initiatives (CNSI), National Institutes of Natural Sciences (NINS) (Grant No. BS261007, BS281002) (Y. H.).

Data Availability The datasets generated and/or analyzed during this study are available from the corresponding authors upon request.

Declarations

Conflict of interest The authors declare no conflicts of interest.

References

- Solter D, Knowles BB (1978) Monoclonal antibody defining a stage-specific mouse embryonic antigen (SSEA-1). *Proc Natl Acad Sci USA* 78:5565–5569
- Bird JM, Kimber SJ (1984) Oligosaccharides containing fucose linked $\alpha(1-3)$ and $\alpha(1-4)$ to N-acetylglucosamine cause decompaction of mouse morulae. *Dev Biol* 104:449–460
- Muramatsu T (1988) Alterations of cell-surface carbohydrates during differentiation and development. *Biochimie* 70:1587–1596
- Toumadje A, Kusumoto K, Parton A, Mericko P, Dowell L, Ma G, Chen L, Barnes DW, Sato JD (2003) Pluripotent differentiation in vitro of murine ES-D3 embryonic stem cells. *In Vitro Cell Dev Biol Anim* 39:449–453
- Capela A, Temple S (2002) LeX/SSEA-1 is expressed by adult mouse CNS stem cells, identifying them as nonependymal. *Neuron* 35:865–875
- Nishihara S, Iwasaki H, Nakajima K, Togayachi A, Ikehara Y, Kudo T, Kushi Y, Furuya A, Shitara K, Narimatsu H (2003) $\alpha 1,3$ -fucosyltransferase IX (Fut9) determines lewis X expression in brain. *Glycobiol* 13:445–455
- Kumar A, Torii T, Ishino Y, Muraoka D, Yoshimura T, Togayachi A, Narimatsu H, Ikenaka K, Hitoshi S (2013) The lewis X-related $\alpha 1,3$ -fucosyltransferase, Fut10, is required for the maintenance of stem cell populations. *J Biol Chem* 288:28859–28868
- Yagi H, Yanagisawa M, Kato K, Yu RK (2010) Lysosome-associated membrane protein 1 is a major SSEA-1-carrier protein in mouse neural stem cells. *Glycobiology* 20:976–981
- Yagi H, Saito T, Yanagisawa M, Yu RK, Kato K (2012) Lewis X-carrying N-glycans regulate the proliferation of mouse embryonic neural stem cells via the notch signaling pathway. *J Biol Chem* 287:24356–24364
- Kudo T, Kaneko M, Iwasaki H, Togayachi A, Nishihara S, Abe K, Narimatsu H (2004) Normal embryonic and germ cell development in mice lacking $\alpha 1,3$ -fucosyltransferase IX (Fut9) which show disappearance of stage specific embryonic antigen 1. *Mol Cell Biol* 24:4221–4228
- Kudo T, Fujii T, Ikegami S, Inokuchi K, Takayama Y, Ikehara Y, Nishihara S, Togayachi A, Takahashi S, Tachibana K, Yuasa S, Narimatsu H (2007) Mice lacking $\alpha 1,3$ -fucosyltransferase IX demonstrate disappearance of lewis x structure in brain and increased anxiety-like behaviors. *Glycobiology* 17:1–9
- Schizophrenia Working Group of the Psychiatric Genomics Consortium (2014) Biological insights from 108 schizophrenia-associated genetic loci. *Nature* 511:421–427
- Goes FS, McGrath J, Avramopoulos D, Wolynec P, Pirooznia M, Ruczinski I, Nestadt G, Kenny EE, Vacic V, Peters I, Lencz T, Darvasi A, Mulle JG, Warren ST, Pulver AE (2015) Genome-wide association study of schizophrenia in Ashkenazi Jews. *Am J Med Genet B* 168:649–659
- Pardiñas AF, Holmans P, Pocklington AJ, Escott-Price V, Ripke S, Carrera N, Legge SE, Bishop S, Cameron D, Hamshere ML (2018) Common schizophrenia alleles are enriched in mutation-intolerant genes and in regions under strong background selection. *Nat Genet* 50:381–389
- Lam M, Chen C-Y, Li Z, Martin AR, Bryois J, Ma X, Gaspar H, Ikeda M, Benyamin B, Brown BC (2019) Comparative genetic architectures of schizophrenia in east Asian and European populations. *Nat Genet* 51:1670–1678
- Yao X, Glessner JT, Li J, Qi X, Hou X, Zhu C, Li X, March ME, Yang L, Mentch FD, Hain HS, Meng X, Xia Q, Hakonarson H, Li J (2021) Integrative analysis of genome-wide association studies identifies novel loci associated with neuropsychiatric disorders. *Transl Psychiatry* 11:69
- Naruse M, Ishino Y, Kumar A, Ono K, Takebayashi H, Yamaguchi M, Ishizaki Y, Ikenaka K, Hitoshi S (2016) The dorsoventral boundary of the germinal zone is a specialized niche for the generation of cortical oligodendrocytes during a restricted temporal window. *Cereb Cortex* 26:2800–2810
- Ishino Y, Hayashi Y, Naruse M, Tomita K, Sanbo M, Fuchigami T, Fujiki R, Hirose K, Toyooka Y, Fujimori T, Ikenaka K, Hitoshi S (2014) Bre1a, a histone H2B ubiquitin ligase, regulates the cell cycle and differentiation of neural precursor cells. *J Neurosci* 34:3067–3307
- Hayashi Y, Nihonmatsu-Kikuchi N, Yu X, Ishimoto K, Hisanaga SI, Tatebayashi Y (2011) A novel, rapid, quantitative cell-counting method reveals oligodendroglial reduction in the frontopolar cortex in major depressive disorder. *Mol Psychiatry* 16:1155–1158
- Molyneaux BJ, Brettler AC, Chen H-H, Hrvatin S, Rinn JL, P, (2015) DeCoN: genome-wide analysis of in vivo transcriptional dynamics during pyramidal neuron fate selection in neocortex. *Neuron* 85:275–288
- Kim D, Pertea G, Trapnell C, Pimentel H, Kelley R, Salzberg SL (2013) TopHat2: accurate alignment of transcriptomes in the presence of insertions, deletions and gene fusions. *Genome Biol* 14:R36
- Liao Y, Smyth GK, Shi W (2014) featureCounts: an efficient general purpose program for assigning sequence reads to genomic features. *Bioinformatics* 30:923–930
- Zhou X, Lindsay H, Robinson MD (2014) Robustly detecting differential expression in RNA sequencing data using observation weights. *Nucleic Acids Res* 42:e91
- Agirman G, Broix L, Nguyen L (2017) Cerebral cortex development: an outside-in perspective. *FEBS Lett* 591:3978–3992
- Garcia-Frigola C, Carreres MI, Vegar C, Herrera E (2007) Gene delivery into mouse retinal ganglion cells by in utero electroporation. *BMC Dev Biol* 7:1–10
- Chaubey S, Wolfe JH (2013) Transplantation of CD15-enriched murine neural stem cells increases total engraftment and shifts

- differentiation toward the oligodendrocyte lineage. *Stem Cells Transl Med* 2:444–454
27. Luque-Molina I, Khatri P, Schmidt-Edelkraut U, Simeonova IK, Hölzl-Wenig G, Mandl C, Ciccolini F (2017) Bone morphogenetic protein promotes lewis x stage-specific embryonic antigen 1 expression thereby interfering with neural precursor and stem cell proliferation. *Stem Cells* 35:2417–2429
 28. Benes FM, Davidson J, Bird ED (1986) Quantitative cytoarchitectural studies of the cerebral cortex of schizophrenics. *Arch Gen Psychiatry* 43:31–35
 29. Chana G, Landau S, Beasley C, Everall IP, Cotter D (2003) Two-dimensional assessment of cytoarchitecture in the anterior cingulate cortex in major depressive disorder, bipolar disorder, and schizophrenia: evidence for decreased neuronal somal size and increased neuronal density. *Biol Psychiatry* 53:1086–1098
 30. Jakobs TC, Ben Y, Masland RH (2003) CD15 immunoreactive amacrine cells in the mouse retina. *J Comp Neurol* 465:361–371

Publisher's Note Springer Nature remains neutral with regard to jurisdictional claims in published maps and institutional affiliations.